arXiv:1505.05954v1 [physics.optics] 22 May 2015

Broadband ultra-high transmission of terahertz radiation through monolayer MoS_2

Xue-Yong Deng[1,2], Xin-Hua Deng[3], Fu-Hai Su[4], Nian-Hua Liu[1,3], Jiang-Tao Liu[1,3*]

[1]Nanoscale Science and Technology Laboratory, Institute for Advanced Study,
Nanchang University, Nanchang 330031, China

[2]School of Materials Science and Engineering, Nanchang University, Nanchang 330031, China

[3] Department of Physics, Nanchang University, Nanchang 330031, China

[4]Key Laboratory of Materials Physics, Institute of Solid State Physics,
Chinese Academy of Sciences, Hefei 230031, Peoples Republic of China

*Email: jtliu@semi.ac.cn

May 25, 2015

Abstract

In this study, terahertz (THz) absorption and transmission of monolayer MoS_2 was calculated under different carrier concentrations. Results showed that the THz absorption of monolayer MoS_2 is very small even under high carrier concentrations and large incident angle. Equivalent loss of the THz absorption is the total sum of reflection and absorption that is one to three grades lower than that of graphene. The monolayer MoS_2 transmission is much larger than that of the traditional GaAs and InAs two-dimensional electron gas. The field-effect tubular structure formed by the monolayer MoS_2-insulation-layer-graphene is investigated. In this structure the THz absorption of graphene to reach saturation under low voltage. Meantime, the maximum THz absorption of monolayer MoS_2 was limited to approximately 5%. Thus, monolayer MoS_2 is a kind of ideal THz Transparent Electrodes.

1 Introduction

Transparent electrode has important prospective applications in the fields of photodetectors, light-emitting diodes (LEDs), vertical cavity surface emitting lasers (VCSELs), and solar cells, et al [1, 2]. As a novel two-dimensional (2-D) material, graphene has high conductivity and very high light transmission within the range of medium infrared and visible light frequency [2–4]. Thus, it is regarded as an ideal transparent electrode material. However, the plasmon of graphene exhibits very high terahertz (THz) absorption when the carrier concentration of graphene is high within the THz or far-infrared frequency range [5–14]. Therefore, graphene with high carrier concentration in THz frequency range is regarded as an absorption medium instead of a transparent electrode.

The frequency of the THz range is mainly the spectrum within 0.1-10 THz. Given its special properties, the spectrum of the THz range has broad applications in communication, medical imaging, radar detection, nondestructive tests, and so on [15, 16]. The transparent electrode within the THz frequency range has important prospective applications in THz detectors, modulators, VCSELs, and phase shifters [5–7, 15–22]. Numerous THz transparent electrodes have been suggested, including two-dimensional electron gas (2DEG), ion-gel, two-dimensional arrays of metallic square holes, graphene with low carrier density, and indium-tin-oxide (ITO) nanomaterials. However, Broadband ultra high transmission THz transparent electrodes is still very desirable.

Recently, another 2-D material, namely, monolayer MoS_2, has attracted much research attention. monolayer MoS_2 has high mobility ($\sim$410 $cm^2V^{-1}s^{-1}$) and excellent mechanical properties [23–34]. However, its optical property is not the same as that of graphene. The monolayer MoS_2 band gap is not zero, which has a high absorption within the visible-light frequency range. This material can be used as a high-efficiency photoelectric detector material instead of an ideal transparent electrode material within the visible light frequency [23–31, 35, 36]. So, the question about whether monolayer MoS_2 can be used to make transparent electrodes within the THz frequency range is interesting.

This study investigated the monolayer $\mathrm{MoS_2}$ absorption and transmission at the THz wave band and compared its results with those of graphene and 2DEG. The results show that monolayer $\mathrm{MoS_2}$ has lower THz absorption than graphene by one to three grades. When the carrier concentration was 10^{12} cm^{-2}, the THz absorption of monolayer $\mathrm{MoS_2}$ was less than 2.4% and its transmission was much higher than that of 2DEG. For example, when the carrier concentration was 8.4×10^{12} cm^{-2}, the relative transmission amplitude of InAs 2DEG was approximately 55%, and the relative transmission amplitude of monolayer $\mathrm{MoS_2}$ could reach 95%. As a representative case, we calculated the field-effect tubular structure formed by monolayer $\mathrm{MoS_2}$-insulation layer-graphene, which would allow the THz of graphene to reach saturation under low voltage. The THz absorption by monolayer $\mathrm{MoS_2}$ was approximately 5% at the maximum.

2 Model and Theory

The experimental results show that the dielectric constant of monolayer $\mathrm{MoS_2}$ within the THz frequency range can be characterized by the Drude model $\varepsilon(\omega) = \varepsilon_\infty - \frac{\omega_p^2}{\omega^2 + i\Gamma\omega}$, where $\omega_p^2 = \frac{Ne^2}{2\varepsilon_0 m^*}$ is the plasma frequency [36]. Within the THz frequency range, the conductivity of graphene can be expressed as [37] $\sigma_g = \frac{e^2}{\pi\hbar}\frac{|\epsilon_F|}{\hbar\Gamma - i\hbar\omega}$, where $\hbar$ is the reduced Planck constant, $\hbar\Gamma = 2.5$ meV is the relaxation rate, ϵ_F is the Fermi level position with respect to the Dirac point, and ω is the angular frequency of the incident THz radiation. The permittivity of graphene can given by $\varepsilon_g(\omega) = 1 + i\frac{\sigma_v}{\omega\varepsilon_0} = 1 + i\frac{\sigma_g}{\omega\varepsilon_0 d_g}$, where ε_0 is the vacuum permittivity, σ_v is the conductivity of bulk materials, and $d_g = 0.34$ nm is the thickness of graphene.

The standard transfer-matrix method was used for the calculation [37, 38]. In the lth layer, the electric field of the TE mode light with incident angle θ_i is given by

$$\mathbf{E}_l(z, y) = \left[A_l e^{ik_{lz}(z-z_l)} + B_l e^{-ik_{lz}(z-z_l)}\right] e^{ik_{ly}y}\mathbf{e}_x, \tag{1}$$

and the magnetic field of the TM mode is given by

$$\mathbf{H}_l(z, y) = \left[A_l e^{ik_{lz}(z-z_l)} + B_l e^{-ik_{lz}(z-z_l)}\right] e^{ik_{ly}y}\mathbf{e}_x, \tag{2}$$

where $k_l = k_{lr} + ik_{li}$ is the wave vector of the light, $\mathbf{e}_x$ is the unit vectors in the x direction, and z_l is the position of the lth layer in the z direction.

The electric fields of TE mode or the magnetic fields of TM mode in the (l+1)th layer are related to the incident fields by the transfer matrix utilizing the boundary condition [37, 38]. Thus, we can obtain the absorbance of lth layer $\mathcal{A}_l$ using the Poynting vector $\mathbf{S} = \mathbf{E} \times \mathbf{H}$ [37, 38]

$$\mathcal{A}_l = [S_{(l-1)i} + S_{(l+1)i} - S_{(l-1)o} - S_{(l+1)o}]/S_{0i}, \tag{3}$$

where $S_{(l-1)i}$ and $S_{(l-1)o}$ [$S_{(l+1)i}$ and $S_{(l+1)o}$] are the incident and outgoing Poynting vectors in (l-1)th [(l+1)th] layer, respectively, S_{0i} is the incident Poynting vectors in air.

3 NUMERICAL RESULTS

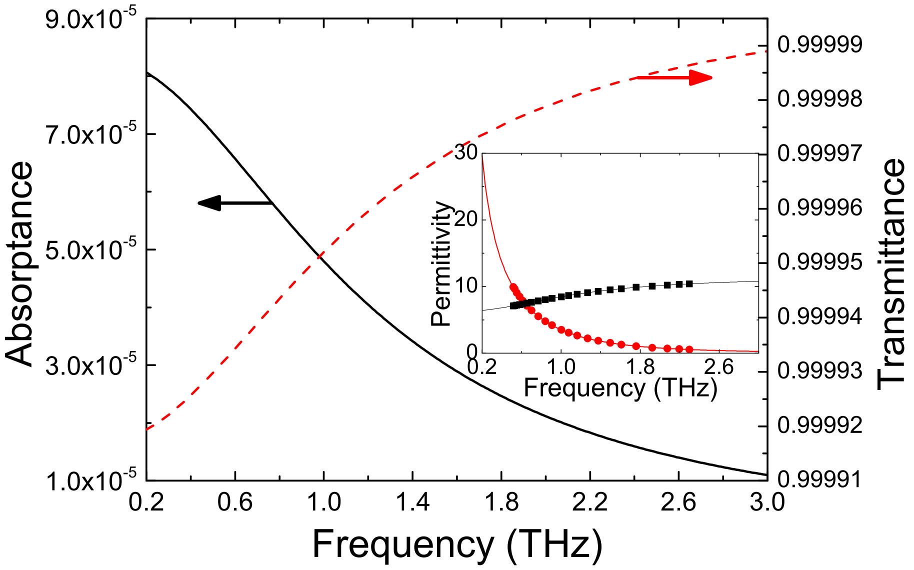

Figure 1: (Color online) The absorption (black solid line) and transmission (red dashed line) of monolayer MoS_2 as they change with the frequency. The inset shows that the dielectric constant of monolayer MoS_2 changes with the wave length, in which the black blocks and red dots are the real and imaginary parts respectively of the dielectric constant measured in the experiment [36]. The black solid and red dashed lines represent the results of fitting.

We calculated the absorption and transmission of monolayer MoS_2 when THz $\omega_p = 16.77$ THz at $N \approx 3.3 \times 10^9$ cm^{-2} (same as the experimental measurement result [36]). The calculation result is indicated in Figure 1. The absorption rate of monolayer MoS_2 was less than 10^{-4}, its reflection rate was even smaller, and the transmission rate was larger than 0.9999. The main reason for this trend is that the effective quality of the monolayer MoS_2 carrier is relatively high, which causes low ion frequency and reduces the absorption of THz waves. Simultaneously, the real and imaginary parts of the monolayer MoS_2 dielectric constant are relatively small (see inset of Figure 1). The thickness of monolayer MoS_2 was very small at approximately 0.65 nm, and thus the monolayer MoS_2 reflection rate and absorption is small. Consequently, monolayer MoS_2 has a very high transmission rate within the THz range.

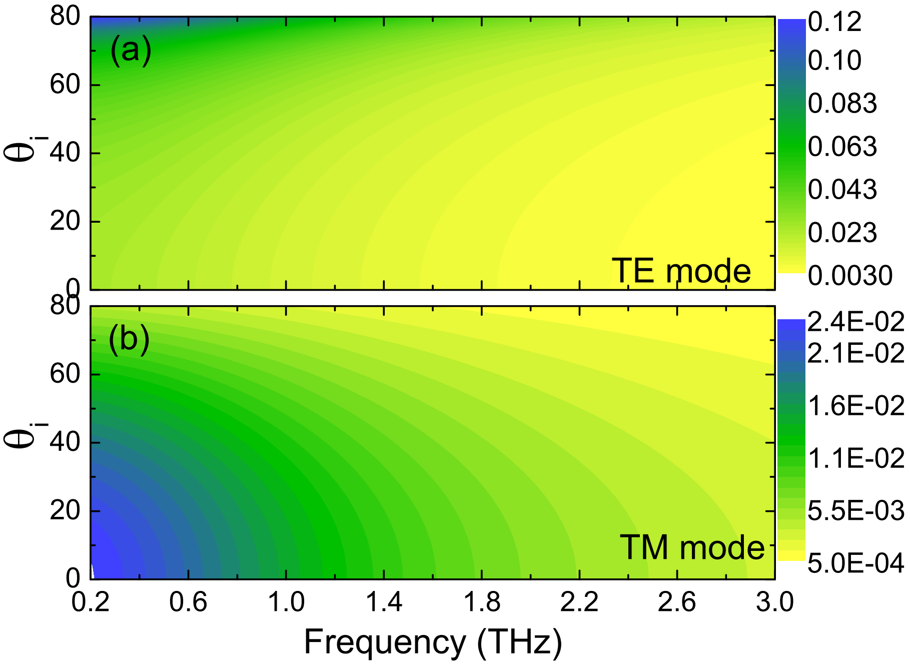

Figure 2: (Color online)Contour plots of the equivalent loss of monolayer MoS_2 as a function of the frequency and the incident angles for the (a) TE and (b) TM modes.

Even for oblique incidence, the monolayer MoS_2 has a very high transmission within the THz range. The equivalent loss (i.e., 1-T, where T is the transmission) of monolayer MoS_2 with carrier concentration 10^{12} cm^{-2} as a function of the frequency and the incident angles for the TE and TM modes are shown in Fig. 2. When the incidence angle θ_i increases, the equivalent loss of TE mode is enhanced and the equivalent loss of TM mode is reduced. But even for TE mode with $\theta_i = 80°$, the equivalent loss is only about 12%.

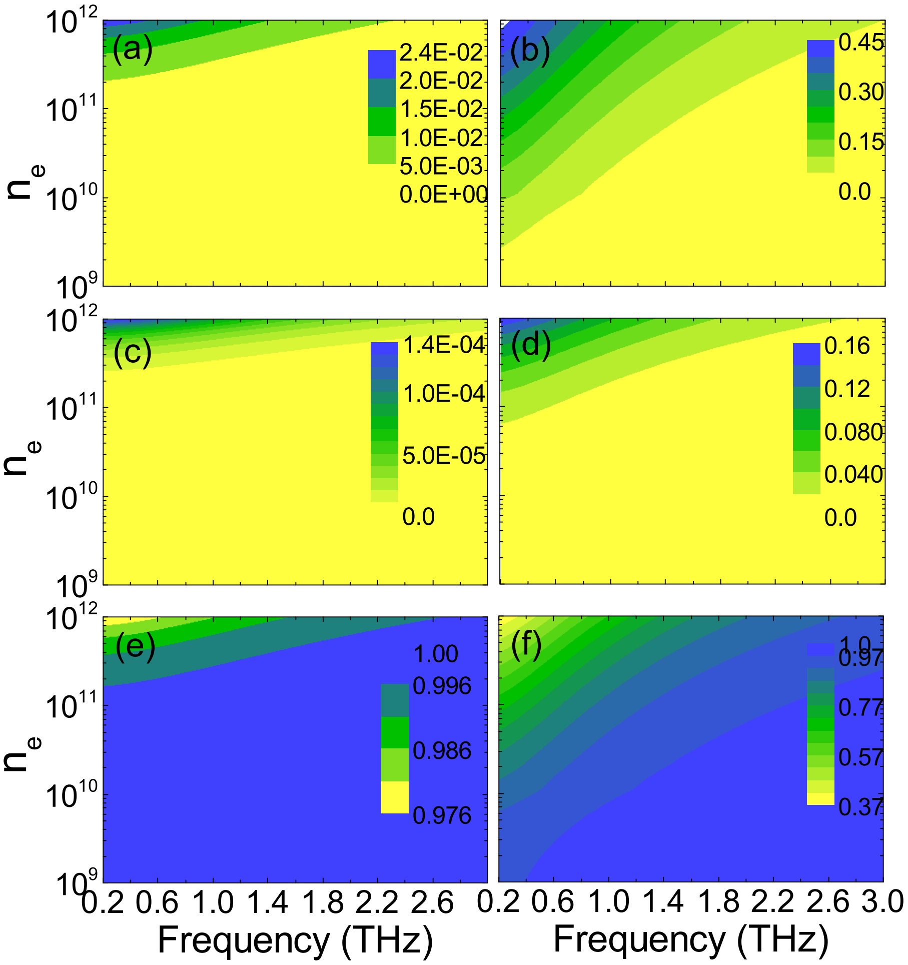

Figure 3: (Color online)contour line diagram of the monolayer MoS_2 absorption (a), reflection (c), and transmission (e), which all change with the frequency and carrier concentration. The contour line diagram of graphene absorption (b), reflection (d), and transmission (f), which all change with the frequency and carrier concentration.

In a real THz device, the electrode usually has high carrier concentration to reduce electrode resistance and increase grid voltage. We studied the THz absorption of monolayer MoS_2, as well as the reflection and transmission under different carrier concentrations. As a point of comparison, we also provided the absorption, reflection, and transmission of graphene. The calculation results are presented in Figure 3. When carrier concentration is increased, the ion frequency and THz absorption of monolayer MoS_2 are increased, whereas the transmission is reduced. According to the Drude modes, the THz absorption of monolayer MoS_2 will decrease with the THz wave frequency. Even when the carrier concentration is at $N = 10^{12}$ cm^{-2}, the wave absorption of monolayer MoS_2 at a frequency of 0.2 THz is only 2.4%. Thus, the reflection can be ignored, and the transmission is larger than 97%. In comparison, when the carrier concentration is at $N = 10^{12}$ cm^{-2}, the wave absorption at the frequency of 0.2 THz by graphene is as high as 46%. Meanwhile, the reflection is 16%, and the transmission is only 37%.

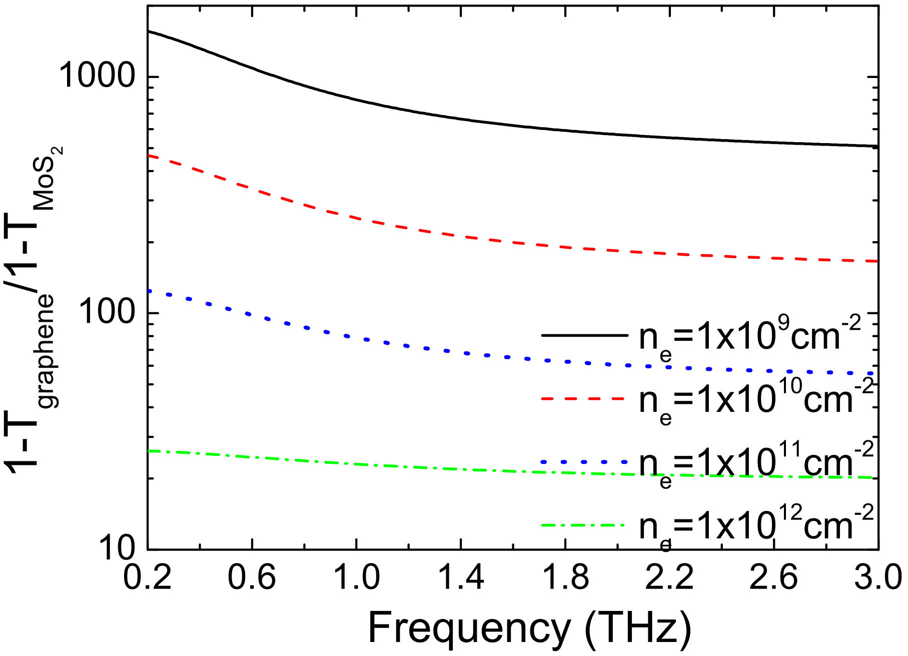

Figure 4: (Color online)The ratio of equivalent loss between monolayer MoS_2 and graphene under different carrier concentrations.

To compare the THz transmission in monolayer MoS_2 and graphene, Figure 4 shows the ratio of equivalent loss between graphene and monolayer MoS_2 (the sum of reflection and absorption). When the carrier concentration is low, such as $N = 10^9$ cm^{-2} and $f = 0.2$ THz, the equivalent loss of monolayer MoS_2 is smaller than 4×10^{-5}, which is three grades smaller that that of graphene. When the carrier concentration is increased, the ratio between graphene and monolayer MoS_2 is reduced. The main reason for this outcome is that even when the carrier concentration is low, such as $N = 10^9$ cm^{-2}, the equivalent loss of graphene is still high, which is approximately 4%. When the carrier concentration is increased, the increase in equivalent loss of graphene is limited, particularly when the carrier concentration is high. Thus, the equivalent loss of graphene is close to saturation.

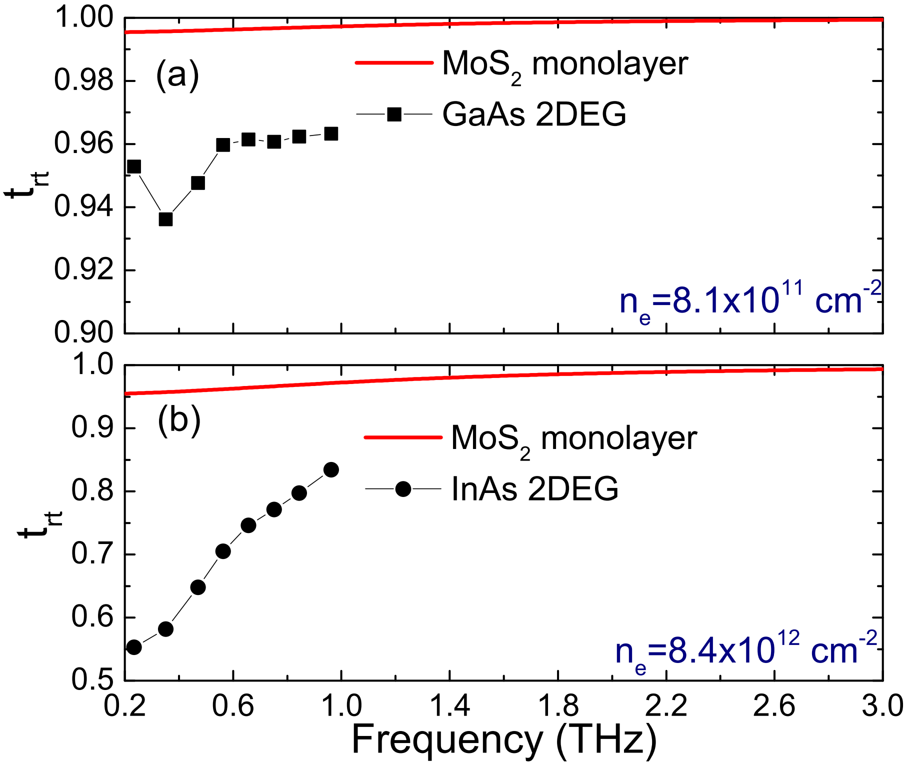

Figure 5: (Color online) the relative transmission amplitude of monolayer MoS_2, and compared with the experimental results of (a) GaAs 2DEG, and (b) InAs 2DEG [39] under different carrier concentrations.

Under actual conditions, the transparent electrode normally remains on the surface of the base. We studied the effect of monolayer MoS_2 on the transmission of samples when it is on the base surface and compared it with the existing experimental results for 2DEG [39]. Thus, the relative transmission amplitude can be defined as $t_{rt} = 1 + n_{sub} + Z_0\sigma_s$. When $N = 8.1\times10^{11}$ cm^{-2}, the relative transmission amplitude of monolayer MoS_2 is still larger than 0.995, whereas in InAs 2DEG, this value is about 0.96 [see Fig. 5 (a)]. When $N = 8.4\times10^{12}$ cm^{-2}, the relative transmission amplitude of monolayer MoS_2 is still larger than 0.95, whereas in InAs 2DEG, this value is only approximately 0.55 [see Fig. 5 (b)]. Given that the change in actual transmission is the norm of the relative transmission amplitude, the effect of monolayer MoS_2 on the transmission is even smaller compared with 2DEG.

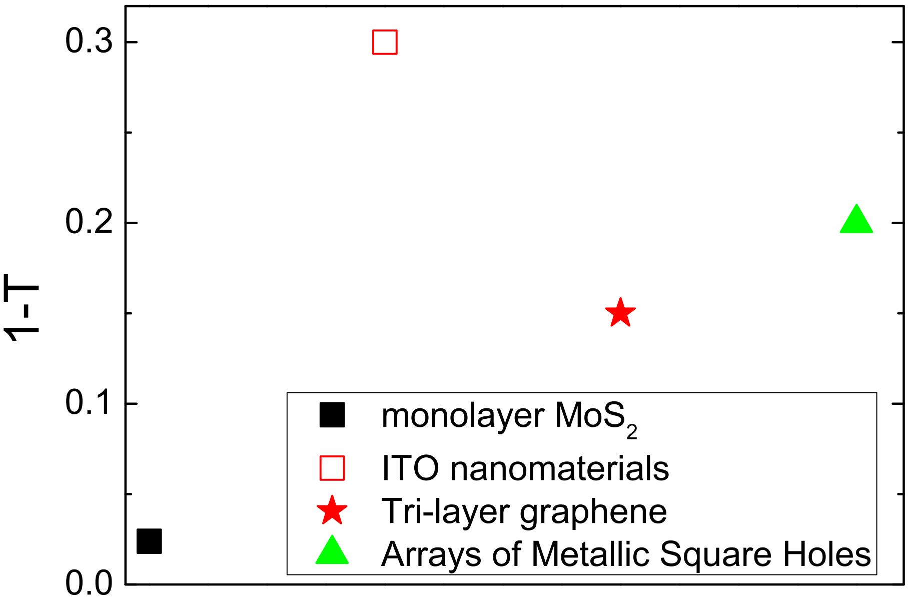

Figure 6: (Color online)The equivalent loss of monolayer MoS_2, two-dimensional arrays of metallic square holes [17], Tri-layer graphene [18], and ITO nanomaterials [19].

Although the details of the transparent electrodes are different, we can still make a comparison with other THz transparent electrodes [Fig. 6]. The maximum equivalent loss of monolayer MoS_2 with $N = 10^{12}$ cm^{-2} is about

2.4%, which is much small than that of the ITO nanomaterials [19] and trilayer graphene [18]. The maximum transmission of two-dimensional arrays of metallic square holes can reach nearly 100%, but the average equivalent loss within broadband frequency regions of the metallic square holes can reach 20% [17].

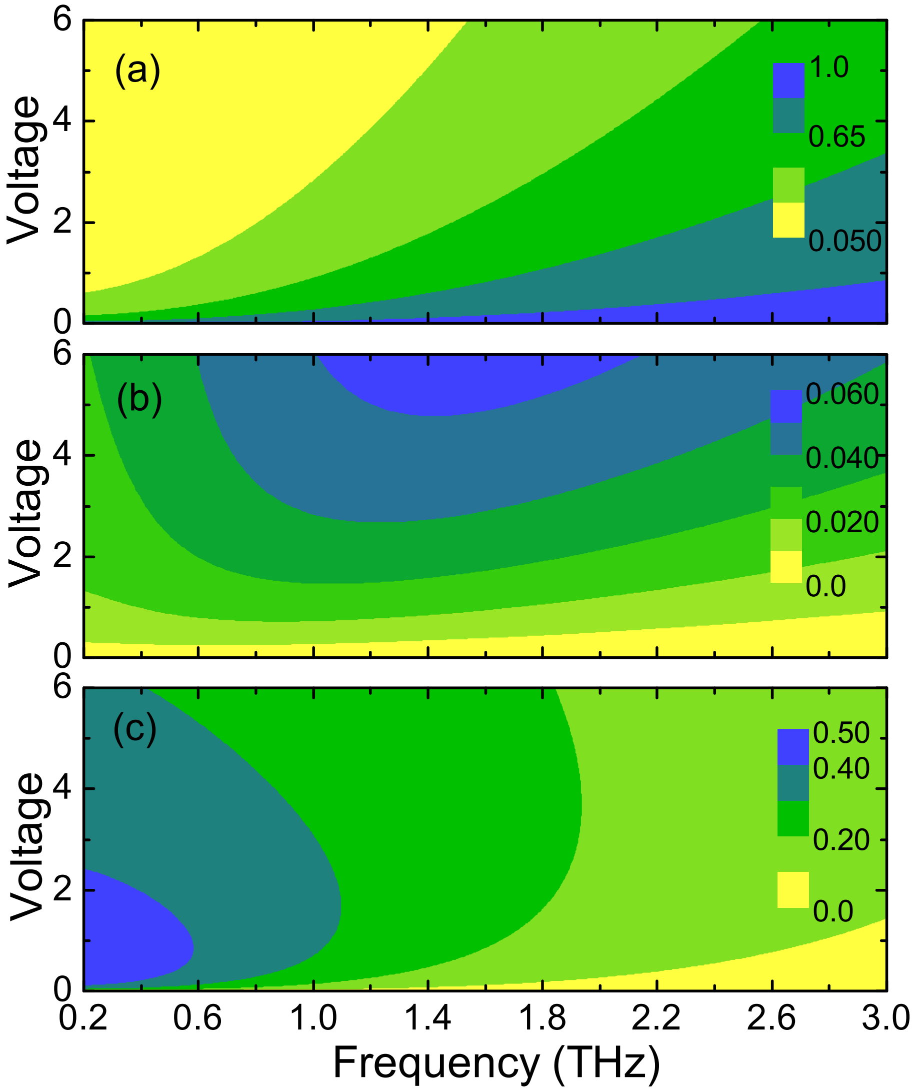

Figure 7: (Color online)the contour line diagram of the (a) total transmission, (b) monolayer MoS_2 absorption, and (c) graphene absorption as a function of the frequency and grid voltage in the sandwich structure.

To reveal the properties of monolayer MoS_2 in real devices, we studied the THz absorption by the field effect formed by monolayer MoS_2-insulation layer-graphene, as well as the regulation effect of the grid voltage between monolayer MoS_2 and graphene on THz. A similar structure was used to make the modem or detector for THz. When the thickness of the insulation layer is smaller, the grid voltage required for modulation will be smaller. But if the thickness of the insulation layer is excessively small, the tunneling current will rapidly increase. The breakdown electric field of the SiO_2 film is relatively strong and can reach 20 MV/cm [40]. In the calculation, the insulation takes 3 nm of the SiO_2 layer. The initial Fermi energy of monolayer MoS_2 and graphene is 0, and the calculation result is illustrated in Figure 7. When the grid voltage is 0, the absorption of THz by monolayer MoS_2 and graphene is very small, and the THz wave is almost completely broken down. When the grid voltage increases, the carrier concentrations of monolayer MoS_2 and graphene are increased and the THz transmission is reduced. When the grid voltage is at 6 V, its transmission is only 5%. However, the maximum absorption of monolayer MoS_2 is only 5.4%. Most of the voltage is absorbed or reflected by graphene. In this structure, the absorption of monolayer MoS_2 and graphene is not at the lowest frequency and the maximum grid voltage because most THz waves are reflected by graphene instead of being absorbed under very high carrier concentration.

4 Conclusions

The study demonstrated that the THz absorption by monolayer MoS_2 is very small over a broadband frequency range even under high carrier concentration and large incident angle. Its equivalent loss is one to three grades smaller than that of graphene. The transmission of monolayer MoS_2 is much larger than that of traditional GaAs or InAs electron gas. We studied the field-effect tubular structure of monolayer MoS_2-insulation layer-graphene, which allows the THz absorption of graphene to reach saturation even under low voltage even while the THz absorption of monolayer MoS_2 is only approximately 5% at the maximum. Therefore, monolayer MoS_2 can be used to make transparent electrodes within the THz frequency range. This development has important prospective applications in optoelectronic devices within the THz frequency range.

References

[1] K. Ellmer, "Past achievements and future challenges in the development of optically transparent electrodes," Nature Photonics **6**, 809–817 (2012).

[2] D. S. Hecht, L. Hu, and G. Irvin, "Emerging transparent electrodes based on thin films of carbon nanotubes, graphene, and metallic nanostructures," Advanced Materials **23**, 1482–1513 (2011).

[3] X. Wang, L. Zhi, and K. Müllen, "Transparent, conductive graphene electrodes for dye-sensitized solar cells," Nano Letter **8**, 323–327 (2008).

[4] S. Bae, H. Kim, Y. Lee, X. Xu, J.-S. Park, Y. Zheng, J. Balakrishnan, T. Lei, H. R. Kim, Y. I. Song, Y.-J. Kim, K. S. Kim, B. Özyilmaz, J.-H. Ahn, B. H. Hong, and S. Iijima, "Roll-to-roll production of 30-inch graphene films for transparent electrodes," Nature Nanotechnology **5**, 574–578 (2010).

[5] L. Ju, B. Geng, J. Horng, C. Girit, M. Martin, Z. Hao, H. A. Bechtel, X. Liang, A. Zettl, Y. R. Shen, and F. Wang, "Graphene plasmonics for tunable terahertz metamaterials," Nature Nanotechnology **6**, 630–634 (2011).

[6] L. Ren, Q. Zhang, J. Yao, Z. Sun, R. Kaneko, Z. Yan, S. Nanot, Z. Jin, I. Kawayama, M. Tonouchi, J. M. Tour, and J. Kono, "Terahertz and infrared spectroscopy of gated large-area graphene," Nano Lett. **12**, 3711–3715 (2012).

[7] B. Sensale-Rodriguez, T. Fang, R. Yan, M. M. Kelly, L. L. Debdeep Jena, and H. G. Xing, "Unique prospects for graphene-based terahertz modulators," Applied Physics Letters **99**, 113104 (2011).

[8] J. Horng, C.-F. Chen, B. Geng, C. Girit, Y. Zhang, Z. Hao, H. A. Bechtel, M. Martin, A. Zettl, M. F. Crommie, Y. R. Shen, and F. Wang,

"Drude conductivity of dirac fermions in graphene," Phys. Rev. B **83**, 165113 (2011).

[9] Z. Z. Zhang, K. Chang, and F. M. Peeters, "Tuning of energy levels and optical properties of graphene quantum dots," Phys. Rev. B **77**, 235411 (2008).

[10] M. Mittendorff, S. Winnerl, J. Kamann, J. Eroms, D. Weiss, H. Schneider, and M. Helm, "Ultrafast graphene-based broadband thz detector," Appl. Phys. Lett. **103**, 021113 (2013).

[11] N. M. R. Peres, Y. V. Bludov, A. Ferreira, and M. I. Vasilevskiy, "Exact solution for square-wave grating covered with graphene: surface plasmon-polaritons in the terahertz range," Journal of Physics: Condensed Matter **25**, 125303 (2013).

[12] Y. Zhou, X. Xu, H. Fan, Z. Ren, J. Bai, and L. Wang, "Tunable magnetoplasmons for efficient terahertz modulator and isolator by gated monolayer graphene," Phys. Chem. Chem. Phys. **15**, 5084–5090 (2013).

[13] X. jun He, T. yue Li, L. Wang, J. min Wang, J. xing Jiang, G. hui Yang, F. yi Meng, and Q. Wu, "Electrically tunable terahertz wave modulator based on complementary metamaterial and graphene," J. Appl. Phys. **115**, 17B903 (2014).

[14] X. Cai, A. B. Sushkov, R. J. Suess, M. M. Jadidi, G. S. Jenkins, L. O. Nyakiti, R. L. Myers-Ward, S. Li, J. Yan, D. K. Gaskill, T. E. Murphy, H. D. Drew, and M. S. Fuhrer, "Sensitive room-temperature terahertz detection via the photothermoelectric effect in graphene," Nature Nanotechnology **9**, 814–819 (2014).

[15] L. Yun-Shik, ed., *Principles of Terahertz Science and Technology* (Springer, New York, 2009).

[16] B. Erik, H. Heinz-Wilhelm, and K. M. FitzGerald, eds., *Terahertz Techniques* (Springer, Berlin, 2012).

[17] G. K. Shirmanesh, E. Yarmoghaddam, A. Khavasi, and K. Mehrany, "Circuit model in design of thz transparent electrodes based on two-dimensional arrays of metallic square holes," IEEE Transactions on Terahertz Science and Technology **4**, 383–390 (2014).

[18] L. Wang, X.-W. Lin, W. Hu, G.-H. Shao, P. Chen, L.-J. Liang, B.-B. Jin, P.-H. Wu, H. Qian, Y.-N. Lu, X. Liang, Z.-G. Zheng, and Y.-Q. Lu, "Broadband tunable liquid crystal terahertz waveplates driven with porous graphene electrodes," Light: Science Applications **4**, e253 (2015).

[19] C.-S. Yang, C.-M. Chang, P.-H. Chen, P. Yu, and C.-L. Pan, "Broadband terahertz conductivity and optical transmission of indium-tin-oxide (ito) nanomaterials," Optics Express **21**, 16670–16682 (2013).

[20] R. Malureanu, M. Zalkovskij, Z. Song, C. Gritti, A. Andryieuski, Q. He, L. Zhou, P. U. Jepsen, and A. V. Lavrinenko, "A new method for obtaining transparent electrodes," Optics Express **20**, 22770–22782 (2013).

[21] Y. Wu, X. Ruan, C.-H. Chen, Y. J. Shin, Y. Lee, J. Niu, J. Liu, Y. Chen, K.-L. Yang, X. Zhang, J.-H. Ahn, and H. Yang, "Graphene/liquid crystal based terahertz phase shifters," Optics Express **21**, 21395–21402 (2013).

[22] C.-S. Yang, T.-T. Tang, P.-H. Chen, R.-P. Pan, P. Yu, and C.-L. Pan, "Voltage-controlled liquid-crystal terahertz phase shifter with indium-ctincoxide nanowhiskers as transparent electrodes," Optics Letters **39**, 2511–2513 (2014).

[23] Q. H. Wang, K. Kalantar-Zadeh, A. Kis, J. N. Coleman, and M. S. Strano, "Electronics and optoelectronics of two-dimensional transition metal dichalcogenides," Nat. Nanotech. **7**, 699–712 (2012).

[24] K. F. Mak, C. Lee, J. Hone, J. Shan, and T. F. Heinz, "Atomically thin MoS_2: a new direct-gap semiconductor," Phys. Rev. Lett. **105**, 136805 (2010).

[25] A. Splendiani, L. Sun, Y. Zhang, T. Li, J. Kim, C. Y. Chim, G. Galli, and F. Wang, "Emerging photoluminescence in monolayer MoS_2," Nano Lett. **10**, 1271–1275 (2010).

[26] O. Lopez-Sanchez, D. Lembke, M. Kayci, A. Radenovic, and A. Kis, "Ultrasensitive photodetectors based on monolayer MoS_2," Nat. Nanotech. **8**, 497–501 (2013).

[27] Z. Yin, H. Li, H. Li, L. Jiang, Y. Shi, Y. Sun, G. Lu, Q. Zhang, X. Chen, and H. Zhang, "Single-layer MoS_2 phototransistors," ACS Nano **6**, 74–80 (2011).

[28] H. S. Lee, S. W. Min, Y. G. Chang, M. K. Park, T. Nam, H. Kim, J. H. Kim, S. Ryu, and S. Im, "MoS_2 nanosheet phototransistors with thickness-modulated optical energy gap," Nano Lett. **12**, 3695–3700 (2012).

[29] W. Choi, M. Y. Cho, A. Konar, J. H. Lee, G. Cha, S. C. Hong, S. Kim, J. Kim, D. Jena, J. Joo, and S. Kim, "High-detectivity multilayer MoS_2 phototransistors with spectral response from ultraviolet to infrared," Adv. Mater. **24**, 5832–5836 (2012).

[30] M. Bernardi, M. Palummo, and J. C. Grossman, "Extraordinary sunlight absorption and one nanometer thick photovoltaics using two-dimensional monolayer materials," Nano Lett. **13**, 3664–3670 (2013).

[31] T. Li and G. Galli, "Electronic properties of MoS_2 nanoparticles," J. Phys. Chem. C **111**, 16192–16196 (2007).

[32] Y. Chen, J. Xi, D. O. Dumcenco, Z. Liu, K. Suenaga, D. Wang, Z. Shuai, Y. S. Huang, and L. Xie, "Tunable band gap photoluminescence from atomically thin transition-metal dichalcogenide alloys," ACS Nano **7**, 4610–4616 (2013).

[33] J. Pu, Y. Yomogida, K. K. Liu, L. J. Li, Y. Iwasa, and T. Takenobu, "Highly flexible MoS_2 thin-film transistors with ion gel dielectrics," Nano Lett. **12**, 4013–4017 (2012).

[34] C. Janisch, N. Mehta, D. Ma, A. L. Elas, N. Perea-Lpez, M. Terrones, and Z. Liu, “Ultrashort optical pulse characterization using WS_2 monolayers,” Opt. Lett. **39**, 383–385 (2014).

[35] C. H. Lui, A. J. Frenzel, D. V. Pilon, Y.-H. Lee, X. Ling, G. M. Akselrod, J. Kong, and N. Gedik, “Trion-induced negative photoconductivity in monolayer mos_2,” Phys. Rev. Lett. **113**, 166801 (2014).

[36] X. Yan, L. Zhu, Y. Zhou, Y. E, L. Wang, and X. Xu, “Dielectric property of mos_2 crystal in terahertz and visible region,” arXiv:1505.03617 (2015).

[37] J. T. Liu, N. H. Liu, L. Wang, X. H. Deng, and F. H. Su, “Gate-tunable nearly total absorption in graphene with resonant metal back reflector,” EPL **104**, 57002 (2013).

[38] J.-T. Liu, T.-B. Wang, X.-J. Li, and N.-H. Liu, “Enhanced absorption of monolayer mos_2 with resonant back reflector,” J. Appl. Phys. **115**, 193511 (2014).

[39] N. A. Kabir, Y. Yoon, J. R. Knab, J.-Y. Chen, A. G. Markelz, J. L. Reno, Y. Sadofyev, S. Johnson, Y.-H. Zhang, and J. P. Bird, “Terahertz transmission characteristics of high-mobility gaas and inas two-dimensional-electron-gas systems,” Appl. Phys. Lett. **89**, 132109 (2006).

[40] C. Sire, S. Blonkowski, M. J. Gordon, and T. Baron, “Statistics of electrical breakdown field in hfo_2 and sio_2 films from millimeter to nanometer length scales,” Appl. Phys. Lett. **91**, 242905 (2007).